# Fault-tolerant Control and Fault Diagnosis of Symmetrical Six-phase Permanent Magnet Synchronous Motor Drives without Controller Reconfiguration

Aihua Liu, Feng Yu, *Member, IEEE,* Qingan Zhu, and Xiaoxin Wu, *Member, IEEE*

***Abstract*—Owing to the multi-degree-of-freedom characteristics and inherent fault-tolerant capacity, six-phase motors have been widely adopted in high-power applications, such as electric vehicle propulsion and aerospace systems. This paper presents the fault-tolerant control strategy of symmetrical six-phase permanent magnet synchronous motor (SSPMSM) under an isolated neutral point topology and proposes a fault diagnosis scheme based on joint diagnosis of multiple variables. First, two mathematical models of SSPMSM and their relationship are established. Subsequently, the current vectors in the torque subspace and harmonic subspace of the two winding sets under fault conditions are analyzed, and the cause of post-fault torque ripple is explained as resulting from controller conflict. In addition, a multivariate fault diagnosis scheme based on voltage threshold in the *x-y* subspace and current trajectory characteristics in the *α-β* subspace is proposed to enhance the diagnostic accuracy. Finally, the feasibility and stability of the proposed control and diagnosis methods are verified by experiments..**

***Index Terms*—Fault-tolerant control, Symmetrical six-phase permanent magnet synchronous motor (SSPMSM), Isolated neutral point, Controller conflict, Multivariate fault diagnosis.**

## I. INTRODUCTION

SIX-PHASE motors possess multiple control degrees of freedom and exhibit inherent advantages in fault tolerance compared to three-phase motors [1]-[3]. Currently, fault-tolerant operation of six-phase motors remains a key research focus, as continuous operational reliability is critically important in many applications [4]. Among different types of faults, winding open circuit faults occur most frequently [5]-[6].

Multi-phase motors can achieve fault tolerance operation without additional hardware [7]. At present, the mainstream fault-tolerant control (FTC) strategies are categorized into three types: minimum copper loss (MCL) [8]-[9], maximum torque (MT) [10]-[11], and full-range minimum copper loss (FRMCL) [12]-[13].

To minimize stator copper losses caused by fault-tolerant operation, many scholars have proposed an FTC strategy based on MCL as a constraint. As presented in [8], the fault-tolerant current is derived under the constraint of minimum stator copper loss, followed by the implementation of deadbeat predictive current control. In [9], the fault-tolerant current is calculated based on the MCL constraint for the nine-phase flux-switching permanent magnet motor, and a corresponding harmonic injection algorithm is designed to achieve the FTC of the motor and mitigate torque ripple.

However, in some applications, it is necessary to maintain a large torque output after fault. Therefore, the FTC strategy with the maximum torque as the optimization objective is studied. In [10], a computationally efficient FTC solution is proposed, which can maximize the average torque, minimize the torque and speed ripple induced by the fault, and is effective under both steady-state and transient operation conditions. In [11], a maximum torque per ampere (MTPA) control strategy is proposed for dual three-phase interior permanent magnet synchronous motors (DT-IPMSM), which can maximize the ratio of average torque to stator current and ensure smooth switching between FTC and health-state control without including significant torque ripple.

Since both MCL and MT adopt a single optimization objective to design FTC strategies, they have certain limitations. Therefore, scholars have studied a FTC strategy that takes into account both, that is, FRMCL. In [12], a full-range minimum losses fault-tolerant strategy is proposed to minimize the stator copper loss while maintaining a high output torque, thereby avoiding secondary faults induced by local overheating. A global optimization strategy based on an online current optimization algorithm is proposed in [13]. Considering fault conditions, MCL and torque ripple-free operation across the full torque range can be achieved without

Manuscript received November 21, 2025; revised December 26, 2025 and January 13, 2026; accepted January 20, 2026. Date of publication March 25, 2026; Date of current version March 4, 2026.

This work was supported in part by the National Natural Science Foundation of China under Grant 52177051, in part by the Postgraduate Research and Practice Innovation Program of Jiangsu Province under Grant SJCX25_2046, and in part by the Key Research Project of Basic Science (Natural Science) in Jiangsu Province under Grant 24KJA470005.

Aihua Liu, Feng Yu, Qingan Zhu, and Xiaoxin Wu are with the School of Electrical Engineering and Automation, Nantong University, Nantong 226019, China. (e-mail: lah@stmail.ntu.edu.cn; yufeng@ntu.edu.cn; 2412310029@stmail.ntu.edu.cn; wu.xx@ntu.edu.cn)

(*Corresponding Author*: *Feng Yu*)

Digital Object Identifier 10.30941/CESTEMS.2026.00002

requiring prior knowledge of the number and location of fault phases.

However, all the aforementioned FTC strategies require closed-loop control of harmonic subspace currents and accurate fault location. Owing to this, some scholars proposed a passive FTC scheme for the open-circuit fault of the winding [14]-[16], which does not need to solve the fault-tolerant current and locate the winding of the fault, which greatly reduces the complexity of the fault-tolerant algorithm. The relevant and valuable researches are listed as follows.

In [14], the causes of abnormal field-oriented control (FOC) prior to fault occurrence are analyzed, followed by the proposal of an FTC scheme that does not require reconstruction of the current reference values. In [15], the fault-tolerant reference current of the *x-y* subspace is obtained according to the open-loop operation of the fault, and a unified fault-tolerant reference current is established accordingly. The smooth switching from fault operation to fault-tolerant operation can be realized without fault location. A natural FTC method based on deadbeat predictive current control (DPCC) was designed in [16], which significantly improved the dynamic performance of the system compared with the traditional FOC. In [17], the direct torque control based on virtual vectors was proposed to eliminate the third and fifth harmonic components in the system and achieve FTC without reconfiguring the controller after a fault, thereby improving the low-speed operation performance of the system. In [18], by studying the offset of the voltage vector after a fault, a universal space vector pulse width modulation (SVPWM) algorithm that can achieve natural fault tolerance was proposed, which solved the problem of designing multiple transformation matrices in traditional methods, reduced the complexity of the algorithm, and decreased the torque ripple after a fault.

In the studies cited above, both conventional FTC and the recently emerging natural FTC require fault diagnosis, prompting extensive research on fault diagnosis algorithms by numerous scholars. In [19], the exact fault occurrence time was determined by monitoring whether the current amplitude in the harmonic subspace exceeded a preset threshold. In [20], an online data-matching-based drive fault diagnosis method was introduced, achieving higher diagnostic accuracy with reduced sample data requirements. Nevertheless, the large data volume and high computational complexity render the method difficult to implement in practical applications.

In view of the above literature review, the traditional FTC needs to solve the fault-tolerant current according to different fault locations, and the corresponding fault diagnosis algorithm is designed to cut into the FTC in real time. This increases the algorithm complexity and the storage space of the program. The proposed natural FTC strategy simplifies the fault-tolerant scheme, but it still needs to design a more complex fault diagnosis algorithm. Therefore, this paper proposes a fault diagnosis algorithm based on multivariate joint diagnosis and the corresponding FTC strategy to improve the stability and security of the system. In this paper, firstly, two mathematical models of symmetrical six-phase permanent magnet synchronous motor (SSPMSM) are presented. Subsequently, a *x-y* subspace open-loop FTC strategy is designed based on the conflict between the two sets of winding torque subspace currents after the fault. Then a fault diagnosis algorithm is developed according to the *α-β* subspace current trajectory and the *x-y* subspace voltage threshold. Finally, an experimental platform is established to verify the proposed control strategy.

The remainder of this paper is organized as follows. First, two mathematical models of SSPMSM and their interrelationship are introduced, followed by an analysis of subspace current characteristics under fault conditions in Section II. Section III presents the current vector expressions in the torque subspace for both winding sets during fault operation, derives the conclusion that controller conflict arises between the harmonic and torque subspaces, and proposes an open-loop FTC strategy. Section IV introduces the fault diagnosis method and corresponding control strategy for the SSPMSM. Experimental validation is conducted in Section V to verify the correctness of the theoretical analysis. Finally, Section VI provides the conclusions and outlook of this study.

## II. The Mathematical Model of SSPMSM

The SSPMSM can be regarded as two sets of three-phase windings with a phase shift of 60°. The universal winding structure of SSPMSM includes common neutral point and isolated neutral point. The topology shown in Fig. 1(a) has no current flowing between the two sets of windings; therefore, there is no need to control the zero-sequence component, which simplifies the control complexity. This paper only studies the isolated neutral point topology as shown in Fig. 2, and gives the performance improvement of the FTC strategy.

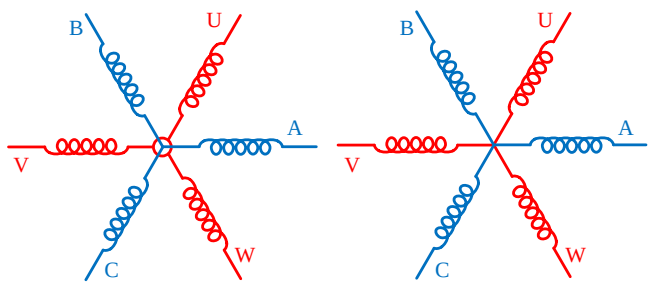


Fig. 1. Different neutral point configurations of SSPMSM. (a) Isolated neutral point. (b) Common neutral point.

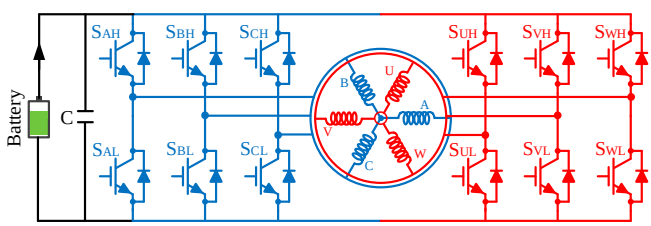


Fig. 2. The isolated neutral point configurations of SSPMSM.

In order to simplify the model of the SSPMSM drive system, the vector space decomposition (VSD) technology is proposed by decoupling the multi-dimensional voltage and current

vectors, and the VSD matrix of SSPMSM is:

$$\boldsymbol{T}_{\mathrm{VSD}}=\frac{1}{3}\begin{bmatrix} 1 & -1/2 & -1/2 & 1/2 & -1 & 1/2 \\ 0 & \sqrt{3}/2 & -\sqrt{3}/2 & \sqrt{3}/2 & 0 & -\sqrt{3}/2 \\ 1 & -1/2 & -1/2 & -1/2 & 1 & -1/2 \\ 0 & -\sqrt{3}/2 & \sqrt{3}/2 & \sqrt{3}/2 & 0 & -\sqrt{3}/2 \\ 1/2 & 1/2 & 1/2 & -1/2 & -1/2 & -1/2 \\ 1/2 & 1/2 & 1/2 & 1/2 & 1/2 & 1/2 \end{bmatrix}\begin{matrix} \alpha \\ \beta \\ x \\ y \\ 0_1 \\ 0_2 \end{matrix} \tag{1}$$

where $\alpha$, $\beta$, $x$, $y$, $0_1$, and $0_2$ represent the subspace components of electrical values such as current and voltage according to VSD. The d-q transformation matrix shown in (2) is further decomposed into DC variable.

$$\boldsymbol{T}_{\mathrm{dq}}=\begin{bmatrix} \cos\theta & \sin\theta & \boldsymbol{0}_{1\times4} \\ -\sin\theta & \cos\theta & \boldsymbol{0}_{1\times4} \\ \boldsymbol{0}_{4\times1} & \boldsymbol{0}_{4\times1} & \boldsymbol{I}_{4\times4} \end{bmatrix} \tag{2}$$

where $\theta$ is electrical angle of PMSM, $\boldsymbol{0}_{4\times1}$ and $\boldsymbol{0}_{1\times4}$ are zero matrices, and $\boldsymbol{I}_{4\times4}$ is a fourth-order unit matrix.

In addition, for the isolated neutral point topology, the motor can also be analyzed by double d-q transformation. The Clark transformation is performed on winding ABC and winding UVW, respectively. After the coordinate transformation, the $\alpha_1$-$\beta_1$ and $\alpha_2$-$\beta_2$ components in the stationary coordinate system can be expressed as (3):

$$\begin{cases} \begin{bmatrix} f_{\alpha1} & f_{\beta1} \end{bmatrix}^{\mathrm{T}}=T_{\alpha\beta1}\begin{bmatrix} f_{\mathrm{A}} & f_{\mathrm{B}} & f_{\mathrm{C}} \end{bmatrix}^{\mathrm{T}} \\ \begin{bmatrix} f_{\alpha2} & f_{\beta2} \end{bmatrix}^{\mathrm{T}}=T_{\alpha\beta2}\begin{bmatrix} f_{\mathrm{U}} & f_{\mathrm{V}} & f_{\mathrm{W}} \end{bmatrix}^{\mathrm{T}} \end{cases} \tag{3}$$

where $\alpha_1$-$\beta_1$ and $\alpha_2$-$\beta_2$ represent the subspace components of electrical values such as current and voltage according to double d-q, $f$ is the current, voltage, and other variables of the motor. The double Clark matrixes $\boldsymbol{T}_{\alpha\beta1}$ and $\boldsymbol{T}_{\alpha\beta2}$ are shown as (4). Then, combined with the Park matrix, the relationship between the subspace components in the double d-q coordinate system and the components in the natural coordinate system can be obtained by Park matrix, respectively.

$$\boldsymbol{T}_{\alpha\beta1}=\frac{2}{3}\begin{bmatrix} 1 & -\frac{1}{2} & -\frac{1}{2} \\ 0 & \frac{\sqrt{3}}{2} & -\frac{\sqrt{3}}{2} \end{bmatrix},\quad \boldsymbol{T}_{\alpha\beta2}=\frac{2}{3}\begin{bmatrix} \frac{1}{2} & -1 & \frac{1}{2} \\ \frac{\sqrt{3}}{2} & 0 & -\frac{\sqrt{3}}{2} \end{bmatrix} \tag{4}$$

According to (3) and (4), it is easy to get the relationship between the double d-q coordinate system and the VSD coordinate, which is also an important prerequisite for the analysis of the subspace current mechanism when the fault is running. The relationship of them is shown as:

$$\begin{cases} f_{\mathrm{d}}=0.5\left(f_{\mathrm{d1}}+f_{\mathrm{d2}}\right) \\ f_{\mathrm{q}}=0.5\left(f_{\mathrm{q1}}+f_{\mathrm{q2}}\right) \\ f_{x}=0.5\left(f_{\mathrm{d1}}-f_{\mathrm{d2}}\right) \\ f_{y}=0.5\left(-f_{\mathrm{q1}}+f_{\mathrm{q2}}\right) \end{cases} \tag{5}$$

The mathematical model of the SSPMSM based on VSD can be established, and corresponding voltages can be presented as:

$$\begin{bmatrix} V_{\mathrm{d}} \\ V_{\mathrm{q}} \end{bmatrix}=R\begin{bmatrix} I_{\mathrm{d}} \\ I_{\mathrm{q}} \end{bmatrix}+\begin{bmatrix} L_{\mathrm{d}} & 0 \\ 0 & L_{\mathrm{q}} \end{bmatrix}\frac{\mathrm{d}}{\mathrm{d}t}\begin{bmatrix} I_{\mathrm{d}} \\ I_{\mathrm{q}} \end{bmatrix}+\omega_{\mathrm{e}}\begin{bmatrix} -L_{\mathrm{q}}I_{\mathrm{q}} \\ L_{\mathrm{d}}I_{\mathrm{d}}+\psi_{\mathrm{f}} \end{bmatrix} \tag{6}$$

$$\begin{bmatrix} V_{x} \\ V_{y} \end{bmatrix}=R\begin{bmatrix} I_{x} \\ I_{y} \end{bmatrix}+\begin{bmatrix} L_{\sigma} & 0 \\ 0 & L_{\sigma} \end{bmatrix}\frac{\mathrm{d}}{\mathrm{d}t}\begin{bmatrix} I_{x} \\ I_{y} \end{bmatrix} \tag{7}$$

where $V_m$ ($m$ = d, q, $x$, $y$) and $I_m$ ($m$ = d, q, $x$, $y$) represent the currents or voltages based on decoupled subspaces of the SSPMSM, respectively; $R$ is stator resistance; $\omega_{\mathrm{e}}$ is electrical angular velocity; $L_{\mathrm{d}}$, $L_{\mathrm{q}}$, and $L_{\sigma}$ are the d-axis, the q-axis, and the stator leakage inductances, respectively; $\psi_{\mathrm{f}}$ is the permanent magnet flux. The electromagnetic torque equation of the SSPMSM in d-q coordinate system can be obtained, as shown in (8):

$$T_{\mathrm{e}}=3p_{\mathrm{n}}I_{\mathrm{q}}\left[I_{\mathrm{d}}\left(L_{\mathrm{d}}-L_{\mathrm{q}}\right)+\psi_{\mathrm{f}}\right] \tag{8}$$

where $p_{\mathrm{n}}$ is the number of pole pairs. Since the dq-axis inductances of the surface-mounted motor are equal, the control method of $i_{\mathrm{d}}=0$ can be adopted.

In order to facilitate the analysis, this paper takes the A-phase open circuit as an example. After the A-phase winding is disconnected, the A-phase current is missing in the current closed-loop, which eventually leads to the current value of each phase no longer balanced. According to the above vector space decoupling theory, the phase current will be changed to (9).

$$I_{\mathrm{A}}=I_{\alpha}+I_{x}+I_{0_1}+I_{0_2}=0 \tag{9}$$

According to Kirchhoff's law, the $0_1$-$0_2$ subspace current is always 0. Hence, both $I_{0_1}$ and $I_{0_2}$ in (9) are 0. Therefore, the subspace current relationship after the open-circuit fault of the A-phase winding can be obtained, as shown in (10), which is caused by physical disconnection.

$$I_{x}=-I_{\alpha} \tag{10}$$

According to (10), it is easy to think that after the open-circuit fault of the winding, the reference value of the original $I_x$ is changed from 0 to $-I_{\alpha}$, and then the proportional resonant (PR) controller is introduced to control it to achieve fault-tolerant operation. However, this kind of traditional fault-tolerant scheme has the following three defects: 1) Due to the resonant characteristics of the PR controller, the parameter tuning process is difficult. 2) For different winding open circuit, fault-tolerant control strategy needs to introduce the corresponding fault-tolerant current reference value, the need for accurate fault diagnosis and location algorithm. 3) The six-phase, twelve-phase and even more multi-phase motors require more pre-stored fault-tolerant current reference values, occupying chip resources. Therefore, this paper proposes a FTC algorithm without fault location, pre-storage of multiple sets of fault-tolerant current reference values, and no current reconstruction to achieve undisturbed operation pre- and post-fault.

## III. The Fault Operation Analysis of SSPMSM

### A. Healthy Operation

When the system is in healthy operation, the output torque of the motor is controlled by controlling the d-q subspace

current. The *x-y* subspace voltage is theoretically 0. However, in the actual system, the motor winding is differentiated and affected by the dead time of the inverter; then, the *x-y* subspace current is inevitably generated. Therefore, if the *x-y* subspace voltage is given to 0 directly during modulation, the harmonic current of the *x-y* subspace cannot be effectively suppressed. Therefore, the *x-y* subspace current closed-loop control is adopted during healthy operation and the reference value is 0.

### *B. Fault Operation*

Taking the open circuit of winding, a winding as an example, the following analysis of the torque component current and harmonic component current generated by the two sets of windings during fault operation is carried out, and the reason for the conflict of the controller is deduced.

Firstly, the symmetrical component method for the three-phase system with star connection is introduced. After the system is unbalanced, the positive sequence component and the negative sequence component will be generated. The angular velocity of the positive sequence component is $\omega_e$, and the angular velocity of the negative sequence component is $-\omega_e$. Therefore, for the three-phase winding where winding A is located, the current vector of the $\alpha$-$\beta$ subspace can be written as:

$$I_{\alpha 1\beta 1} = I_{p1}e^{j(\omega_e t+\theta_{p1})} + I_{n1}e^{j(-\omega_e t-\theta_{n1})} \tag{11}$$

where $\omega_e$ is electrical angular velocity; $I_{p1}$ and $\theta_{p1}$ are the amplitude and phase of the positive sequence component, respectively. Similarly, $I_{n1}$ and $\theta_{n1}$ are the amplitude and phase of the negative sequence component, respectively. Additionally, $I_{\alpha 1\beta 1}$ is $\alpha$-$\beta$ subspace current of ABC. Park transformation is performed on both sides of (11), respectively. The d-q component of the first set of windings is obtained, as shown in (12).

$$I_{d1q1} = I_{p1}e^{j\theta_{p1}} + I_{n1}e^{j(-2\omega_e t-\theta_{n1})} \tag{12}$$

where $I_{n1}e^{j(-2\omega_e t-\theta_{n1})}$ is the double frequency negative sequence component generated in the d-q subspace after the winding A fault. $I_{p1}e^{j\theta_{p1}}$ is DC component in d-q subspace. Since the isolated neutral point topology is adopted in this paper, the winding current can be analyzed by combining the double d-q and VSD theory. The relationship between the two is as (10) after the fault occurs, and under the dual action of d-q closed-loop and *x-y* closed-loop, there may be two cases.

*1) The d-q Closed-loop is Enabled with Priority*

From the perspective of decoupling, the d-q subspace current is obtained by superimposing the torque subspace currents of two sets of windings. In order to maintain the d-q subspace current without ripple pulsation after the fault, the AC harmonic component in the torque subspace of the second set of windings, that is, the $d_2$-$q_2$ subspace, should cancel each other out with the AC component in the first set of windings. Therefore, the torque subspace current $I_{d2q2}$ of the second set of windings can be obtained as:

$$I_{d2q2} = I_{p2}e^{j\theta_{p2}} - I_{n1}e^{j(-2\omega_e t-\theta_{n1})} \tag{13}$$

where $I_{p2}e^{j\theta_{p2}}$ is DC component in d-q subspace of UVW.

According to (5), (12), and (13), the current of d-q subspace and *x-y* subspace of SSPMSM in VSD coordinate system can be obtained as shown in (14).

$$\begin{cases} I_{dq} = 0.5\left(I_{p1}e^{j\theta_{p1}} + I_{p2}e^{j\theta_{p2}}\right) \\ I_{xy} = 0.5\left(I_{p1}e^{j\theta_{p1}} - I_{p2}e^{j\theta_{p2}}\right)^* + I_{n1}e^{j(2\omega_e t+\theta_{n1})} \end{cases} \tag{14}$$

*2) The x-y Closed-loop is Enabled with Priority*

The *x-y* subspace current reflects the difference between the two sets of winding currents. Therefore, if the harmonic plane is to be controlled to be constant, the AC component in the d-q subspace current of the second set of windings should be equal to that of the first set of windings. Thus, the $d_2$-$q_2$ subspace current can be obtained as

$$I_{d2q2} = I_{p2}e^{j\theta_{p2}} + I_{n1}e^{j(-2\omega_e t-\theta_{n1})} \tag{15}$$

Similarly, according to (5), (12), and (15), the current of d-q subspace and *x-y* subspace of SSPMSM in VSD coordinate system can be written as:

$$\begin{cases} I_{dq} = 0.5\left(I_{p1}e^{j\theta_{p1}} + I_{p2}e^{j\theta_{p2}}\right) + I_{n1}e^{j(-2\omega_e t-\theta_{n1})} \\ I_{xy} = 0.5\left(I_{p1}e^{j\theta_{p1}} - I_{p2}e^{j\theta_{p2}}\right)^* \end{cases} \tag{16}$$

According to the above derivation, especially the comparative analysis of (14) and (16), the controller will generate conflicting subspace currents in order to achieve different control objectives. Therefore, the two control objectives cannot be achieved at the same time. After the open-circuit fault of the winding occurs, there is a serious imbalance between the two sets of windings of the motor, so the actual current of the *x-y* subspace cannot be controlled to 0. Therefore, it can be concluded that in order to ensure the same torque output capacity and low torque ripple performance after the fault, it is necessary to solve the conflict between the d-q subspace and the *x-y* subspace current closed-loop controller.

In this paper, the open-loop FTC strategy is proposed, which is to disconnect the current closed loop of the *x-y* subspace after the fault, and directly set the voltage reference value of the *x-y* subspace to 0, thus avoiding the conflict between the torque subspace and the harmonic subspace. Under this condition, the harmonic subspace still has the current generated by the open circuit fault, such that the winding A open circuit will generate the current in (10).

## IV. THE FAULT DIAGNOSIS AND CONTROL STRATEGY

After discussing the FTC algorithm in Section III, it is also very important to study the fault diagnosis of the system. Based on the proposed fault-tolerant strategy, two fault diagnosis algorithms are designed and tested at the same time, which can effectively improve the robustness of the system and reduce the risk of false diagnosis.

### *A. Fault Diagnosis based on x-y Subspace Voltage Threshold*

According to the VSD theory, the current component in the *x-y* subspace increases significantly after fault. At this time,

the *x-y* subspace voltage will produce a larger value of *x-y* subspace voltage. Therefore, a simple fault diagnosis algorithm for *x-y* subspace voltage threshold can be designed. During the operation of the SSPMSM, the output value of the *x-y* subspace current closed-loop is detected at all times. In order to avoid the misdiagnosis caused by normal fluctuations, a simple filtering process is performed on the obtained detection value. Then, compared with the preset threshold $u_{xy\_max}$, if it exceeds the preset value in both electrical cycles and satisfies (17), it is judged that the winding open circuit fault occurs in the motor.

$$\begin{cases} u_x \geq u_{xy\_max} \\ u_y \geq u_{xy\_max} \end{cases} \tag{17}$$

where $u_{xy\_max}$ is fault threshold. In this method, it is difficult to select the threshold $u_{xy\_max}$. For different power levels and different types of motors, different thresholds need to be adopted.

### *B. Fault Diagnosis based on α-β Subspace Current Trajectory*

It can be known from the VSD theory that the *α-β* subspace current is the sine wave with the phase difference of 90° and equal amplitude when the SSPMSM is in healthy operation. Therefore, the current trajectory of the *α-β* subspace is the standard circle, and the radius of the circle is equal to the current *q*-axis current value. When the winding open circuit fault occurs, the phase current imbalance increases, and the *α-β* subspace current is no longer balanced, so its trajectory also changes from circular to elliptical. The phase current of SSPMSM is collected in real time, and the real-time value of *α-β* subspace current is obtained according to the VSD transformation and stored as ($I_{\alpha 0}$, $I_{\beta 0}$), so the tangent equation of this point is shown in (18) when the motor is running healthily. However, when the motor faults, the current trajectory of the *α-β* subspace becomes an ellipse with the long half axis equal to $I_q$ and the short half axis equal to 0.5 $I_q$. Therefore, the tangent equation at this time is (19).

$$I_\alpha \cdot I_{\alpha 0} + I_\beta \cdot I_{\beta 0} = I_q^2 \tag{18}$$

$$4I_\alpha \cdot I_{\alpha 0} + I_\beta \cdot I_{\beta 0} = I_q^2 \tag{19}$$

In each control cycle, the *α*-axis current value $I_{\alpha 0}$ is calculated according to the phase current obtained by sampling, and then the $I_{\beta 1}$ and $I_{\beta 2}$ are solved by (18) and (19) respectively. Under the two tangent equations, two values with large difference will be obtained. Then, $I_{\beta 1}$ and $I_{\beta 2}$ are compared with the actual *β*-axis current value $I_{\beta 0}$ respectively. If $I_{\beta 1}$ is closer to $I_{\beta 0}$, it is in healthy operation at this time. If $I_{\beta 2}$ is closer to $I_{\beta 0}$, it is judged as a fault at this time.

This method can be directly applied to any motor without determining the *x-y* subspace voltage preset threshold. However, when the load changes abruptly, due to the rapid change of $I_q$, it may lead to misdiagnosis. Therefore, it needs to be combined with the first fault diagnosis method. Only when both methods are judged to be faulty, the system will disconnect the *x-y* subspace current closed-loop.

### *C. Control Strategy of Fault Diagnosis and Fault-tolerant*

The following briefly introduces the control flow of SSPMSM fault-tolerant operation and fault diagnosis based on Fig. 3. As shown in Fig. 3(a), the multi-variable joint fault diagnosis algorithm proposed in this paper is demonstrated. On one hand, by judging whether the *x-y* subspace voltage exceeds the set threshold, it is determined whether the fault occurs. On the other hand, by solving the current value of the *α-β* subspace at each moment in the operation of the motor, and according to the tangent equation of the current trajectory of the *α-β* subspace under different operating conditions, it is judged whether the flux linkage runs in the circular state or the elliptical state, and finally the fault flag is obtained. It should be emphasized that two methods must be used to obtain the fault flag at the same time to determine that the system is really faulty and then switch to open-loop FTC.

Then, the overall control block diagram is introduced. Firstly, for healthy operation, the speed is closed-loop controlled. The output of the speed close-loop is the given value of the q-axis current to control the torque output of the motor. In addition, in order to avoid the excess loss of the system, the d-axis current is controlled to 0. For the *x-y* subspace current loop, when the system is in healthy operation, the reference voltages $u_x^*$ and $u_y^*$ of the *x-y* subspace current closed-loop control output are used as the input of SVPWM, which can effectively suppress the generation of current harmonics and reduce the operating loss. When the winding open-circuit fault occurs, the *x-y* subspace current closed-loop is disconnected, and the $u_{xy}^*$ are is directly given to be 0, and it is sent to the modulation module for calculation to eliminate the controller conflict and reduce the torque ripple after the fault.

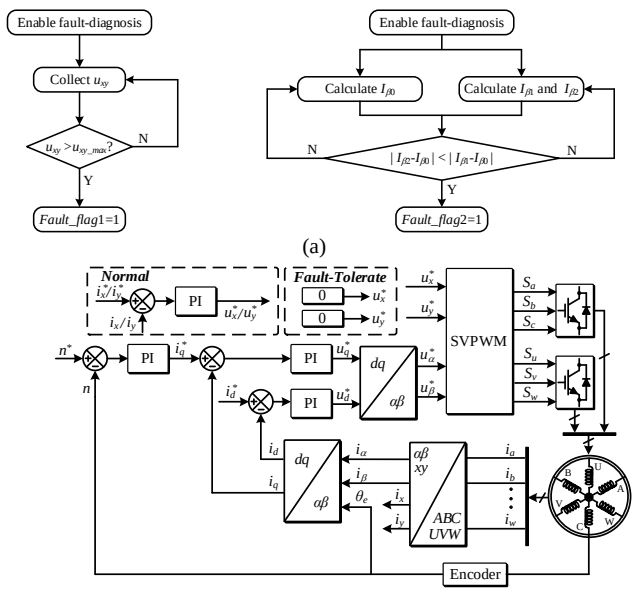


Fig. 3. Controller diagram for both pre- and post-fault operations. (a) Fault-diagnosis. (b) Healthy and FTC strategy.

## V. EXPERIMENTAL VERIFICATION

In order to verify the FTC and fault diagnosis algorithm proposed in this paper, the experimental verification is carried out on the experimental platform shown in Fig. 4. There are

seven current sensors and a voltage sensor used as measurement. The current sensor is used to measure the motor winding current and the DC current, and the voltage sensor is used to measure the DC bus voltage. The module has a withstand voltage of 1200 V and uses a 15 V voltage to ensure that it is reliably driven. In addition, Texas Instruments' digital signal processor TMS320F28335 is used to process sampling signals and implement drive control algorithms. Finally, the parameters of the SSPMSM used in this experiment are shown in Table I.

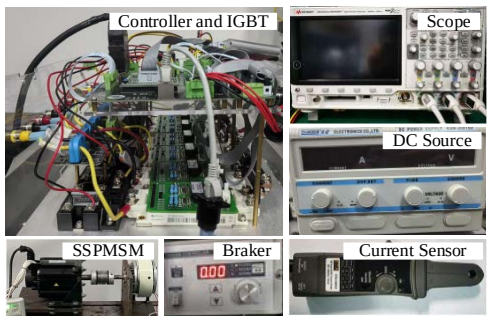


Fig. 4. Experimental test rig.

TABLE I
PARAMETERS OF EXPERIMENTAL PLATFORM

| Parameters | Value |
|---|---|
| Pole pairs | 5 |
| d-axis inductance/mH | 8 |
| q-axis inductance/mH | 8 |
| PM flux/Wb | 0.042 |
| Rated speed/(r/min) | 1000 |
| Rated torque/(N · m) | 5 |
| Rated current/A | 10 |

### A. *Healthy-fault Operation*

Firstly, the switching process of SSPMSM from healthy operation to A-phase disconnection operation under isolated neutral point topology is analyzed. The experimental results are shown in Fig. 5. After the fault occurs, since the current cannot flow in the winding A, according to Section III, $I_x = -I_\alpha$ at this time. In addition, since $I_y$ is independent of winding A, $I_y$ does not change. Then, by observing the *x*-*y* subspace voltage, it can be known that after the fault, due to the conflict of the controller and the physical change of the actual value of the *x*-axis, it cannot track the reference value, so $u_x$ is out of control. Because the limiting setting of the *x*-*y* subspace voltage is small when designing the controller, a waveform similar to a rectangular wave is presented. Similarly, since the *y*-axis is independent of the winding A, the $u_y$ is not affected.

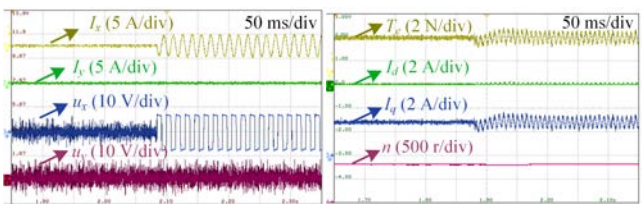


Fig. 5. Healthy to fault operation. (a) *x*-*y* subspace current and voltage. (b) Torque and speed of SSPMSM, d-q subspace current.

As shown in Fig. 5(b), after the open-circuit fault of the motor winding occurs, on one hand, the winding current after the motor phase is broken produces an extremely serious imbalance. On the other hand, the conflict between the physical immutability of $I_x$ and its reference value aggravates the torque ripple.

### B. *Fault-fault-tolerant Operation*

Before verifying the fault diagnosis algorithm, the FTC performance is verified by experiments. Figs. 6(a)–6(c) are tthe motor switching process from A-phase open-circuit fault operation to *x*-*y* subspace open-loop fault-tolerant operation. It can be clearly seen that after switching to open-loop control, the *x*-*y* subspace current loop is released, and the conflict between the torque subspace current loop is resolved. Therefore, compared with the fault operation, the torque ripple of the motor is reduced by 50%, and the excellent FTC performance is obtained. In addition, it can be seen from the figure that the d-axis current ripple is also reduced a lot. This is because the projection of the torque subspace current on the d-axis decreases with the release of the *x*-*y* subspace current loop.

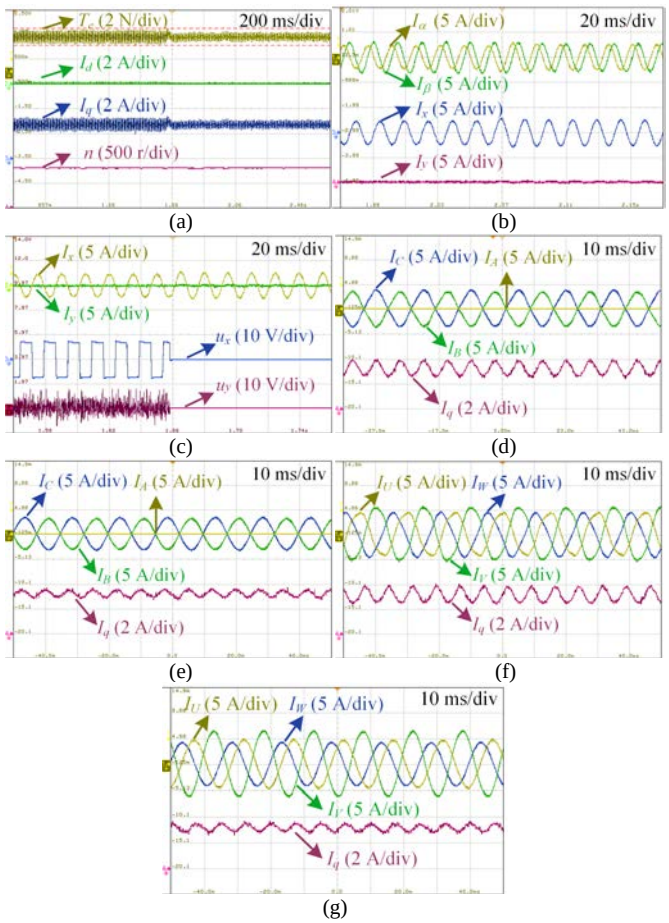


Fig. 6. The result of fault-tolerant operation. (a) Torque and speed of SSPMSM, d-q subspace current. (b) *α*-*β* and *x*-*y* subspace currents. (c) *x*-*y* subspace current and voltage. (d) Phase current $I_A$, $I_B$, $I_C$, and q-axis current under fault operation. (e) Phase current $I_A$, $I_B$, $I_C$, and q-axis current under fault-tolerant operation. (f) Phase current $I_U$, $I_V$, $I_W$, and q-axis current under fault operation. (g) Phase current $I_U$, $I_V$, $I_W$, and q-axis current under fault-tolerant operation.

During the switching process from fault to fault-tolerant operation, the $\alpha$-$\beta$ and $x$-$y$ subspace currents are shown in Fig. 6(b). It can be clearly seen that during the fault operation, the torque subspace current shows a serious imbalance, and the motor cannot produce a standard circular magnetomotive force. However, after the FTC is involved, the torque subspace current is rebalanced and a circular magnetomotive force is generated.

In addition, in the case of fault and fault-tolerant operation, the current of $I_x$ is equal to $-I_\alpha$, and $I_y$ is not affected by the open circuit of winding A, which also verifies the conjecture of Section III. In addition, Fig. 6(c) shows the $x$-$y$ subspace current and voltage from fault to fault-tolerant operation, and the current and voltage of the $x$-axis are analyzed here. When the FTC strategy is not cut in, $I_x$ shows some distorted sinusoidal current. After the open-loop control of the $x$-$y$ subspace, $I_x$ becomes a standard sinusoidal current and the amplitude is larger than before. This is because when the fault is running, a part of the harmonic component is transferred to the d-q subspace, and after the controller conflict is resolved, the harmonic current is completely returned to the $x$-axis. In addition, Figs. 6(d) and 6(f) show the phase current waveforms of the motor during fault operation. It can be clearly seen that the current is no longer sinusoidal and has obvious distortion. Then, Figs. 6(e) and 6(g) show the phase current waveforms after fault tolerance. After the controller conflict is released, the current waveform distortion disappears and returns to sine.

To more comprehensively demonstrate the advantages of the fault-tolerant method proposed in this paper over traditional methods, the following section takes the MCL FTC strategy as an example for comparison. Fig. 7 shows the switching process of the motor from healthy operation to fault operation to fault-tolerant operation under the MCL strategy. When it needs to be explained, the operating conditions are consistent with the waveform shown in the manuscript, including voltage, load, speed, etc. In the VSD theory, if the system is connected to an isolated neutral point topology, the relationship between the A-phase current and the subspace is shown in (9). At this time, the MCL is taken as the optimization objective. Obviously, $I_x$ has only the unique solution $-I_\alpha$. Therefore, in this mode, the reference value of $I_x$ in the original healthy operation is changed from 0 to $-I_\alpha$ to achieve the minimum loss FTC.

Then, comparing Fig. 7 with Figs. 5 and 6 in the manuscript, there is no significant difference between the two control methods in reducing torque and speed ripple. In addition, both the MCL strategy and the strategy mentioned in the manuscript show very close subspace currents, which indicates that the open-loop FTC can achieve the same effect as the harmonic plane current closed-loop control in terms of copper loss and torque ripple. However, the method introduced in this paper does not need to calculate the fault-tolerant current reference in advance, nor does it need to design a PR controller for controlling the alternating current, which is the biggest advantage of the traditional FTC method.

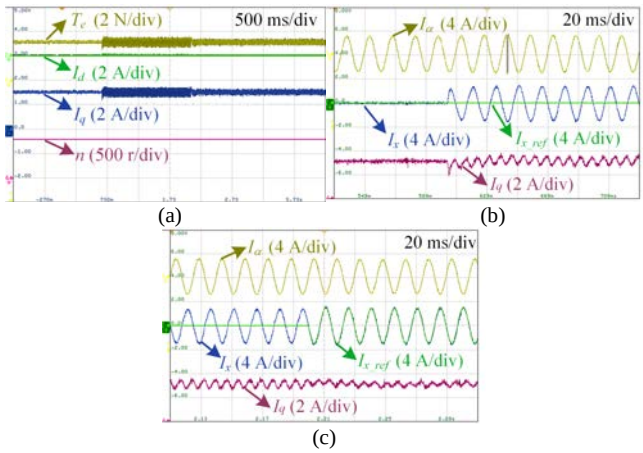


Fig. 7. The result of fault-tolerant operation with MCL strategy. (a) Torque and speed of SSPMSM, d-q subspace current. (b) $I_\alpha$, $I_q$, $I_{x\_ref}$, and $I_x$ from healthy to fault operation. (c) $I_\alpha$, $I_q$, $I_{x\_ref}$, and $I_x$ from fault to fault-tolerant operation.

According to the natural FTC method described in [14], it was applied to SSPMSM in this manuscript, and the experimental results are shown in Fig. 8. It can be seen that since neither of the two methods requires fault location but only simple diagnosis, both can quickly switch to FTC after a fault occurs. In addition, due to the addition of closed-loop control in the $x$-$y$ subspace in [14], better torque performance can be achieved. However, two PR controllers have also been added, while the method adopted in this paper does not require this step, further simplifying the system complexity and enhancing reliability.

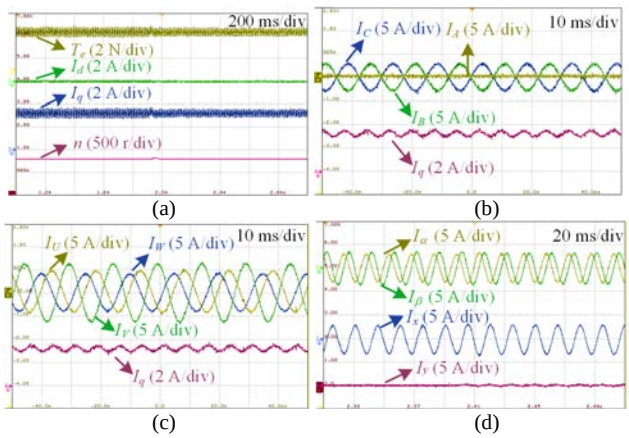


Fig. 8. The result of fault-tolerant operation in [14]. (a) Torque and speed of SSPMSM, d-q subspace current. (b) Phase current $I_A$, $I_B$, $I_C$, and q-axis current under fault-tolerant operation. (c) Phase current $I_U$, $I_V$, $I_W$, and q-axis current under fault-tolerant operation. (b) $\alpha$-$\beta$ and $x$-$y$ subspace currents.

### *C. x-y Subspace Closed-loop or Open-loop*

According to the above experimental verification, disconnecting the $x$-$y$ subspace current closed-loop after the fault can effectively solve the conflict between the subspace currents. Therefore, it can be imagined that in order to simplify the complexity of the system, the following section is to verify whether the open-loop control strategy is more advantageous in the healthy state of the SSPMSM. Figs. 9(a) and 9(b) show the experimental results of the closed-loop switching from the $x$-$y$ subspace current to the open-loop

operation in the healthy state. It can be seen from the torque and speed waveforms in Fig. 9(a) that there is almost no change between the two before and after switching. Therefore, no matter the *x-y* subspace current open-loop operation or closed-loop operation, it has no effect on the output performance of the motor. However, it can be seen from Fig. 9(b) that the *y*-axis current fluctuates after both $u_x$ and $u_y$ are given to 0. This is mainly due to the fact that the motor windings cannot be completely consistent. Therefore, if the *x-y* subspace current is not closed-loop controlled, even if the default current loop output is 0 during modulation, the actual *x-y* subspace current is not suppressed, which will cause system loss and is not conducive to high-efficiency operation. Therefore, in healthy operation, the *x-y* subspace current closed-loop operation is still used.

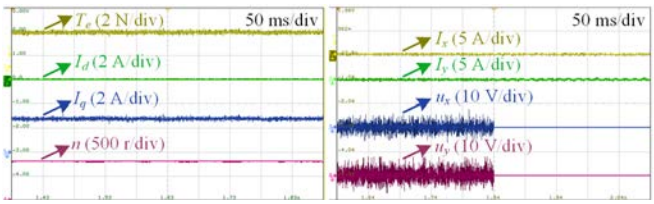


(a) (b)

Fig. 9. Operation from *x-y* closed-loop to open-loop. (a) Torque and speed of SSPMSM, d-q subspace current. (b) *x-y* subspace current and voltage.

### D. Fault Diagnosis

Firstly, the diagnostic method based on *x-y* subspace voltage threshold is experimentally verified, and $u_{xy\_max}$ is selected as 1, 4, and 10, respectively. The *Fault_flag*1 and *Fault_flag*2 are fault diagnosis results. The results are shown in Fig. 10(a), because the threshold value is too small, even if no open-circuit fault occurs, the voltage fluctuation of the *x-y* subspace is enough to make it diagnosed as a fault. However, a larger threshold is selected in Fig. 10(e), which will cause another problem. Even if a fault occurs, the *x-y* subspace voltage always fails to reach the threshold. In Fig. 10(c), a compromise value is selected as the judgment threshold. After the fault occurs, the fault occurrence time is quickly judged and the FTC is quickly cut in. Therefore, for this fault diagnosis method, the voltage threshold selection of the *x-y* subspace is extremely important.

Fig. 10(b) shows the experimental results of the fault diagnosis algorithm based on the tangent equation. When the fault occurs, the q-axis loses its activity, resulting in the deviation of the flux circle trajectory. Therefore, the fault can be determined quickly by judging the difference between $I_{\beta 2}$ and $I_{\beta 0}$. However, this method is sensitive to changes in the external characteristics of the system. When the load changes or the speed changes, the diagnostic marker may be triggered, and there is a risk of misdiagnosis. Fig. 10(d) shows the switching process of the reference speed from 800 to 400 r/min, and the second method has a false diagnosis. Fig. 10(g) shows the switching process of the load torque from 3 to 0 N·m, and only also the second method has a false diagnosis. Therefore, combining the two methods to diagnose at the same time, as shown in Fig. 10(f), it is neither necessary to carefully select the voltage threshold of the *x-y* subspace, nor to worry about the risk of misdiagnosis caused by a single variable.

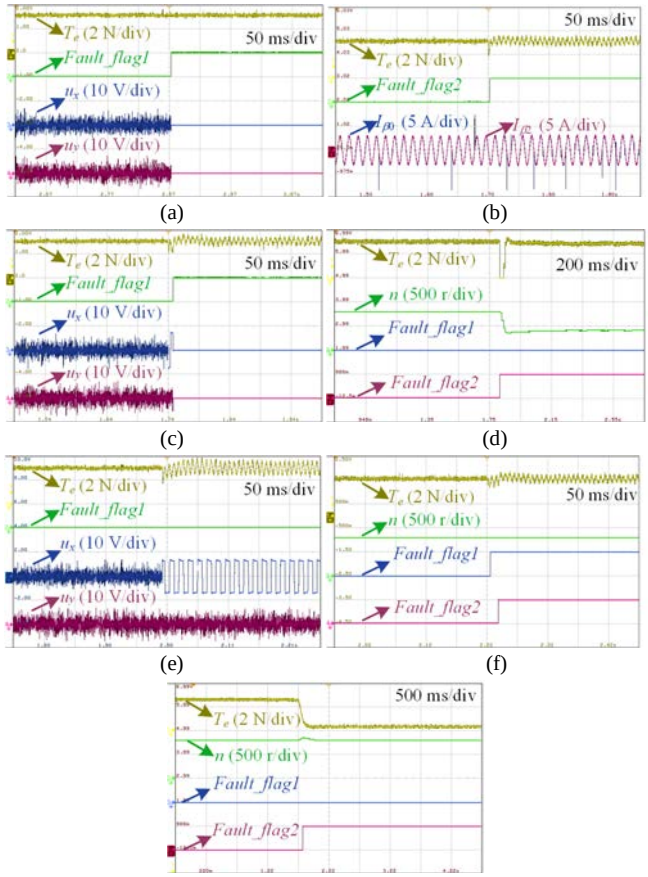


(a) (b) (c) (d) (e) (f) (g)

Fig. 10. Fault diagnosis. (a) Torque, *x-y* subspace voltage, and *Fault_flag1* under $u_{xy\_max}$ = 1. (b) Torque, $I_{\beta 0}$, $I_{\beta 2}$, and *Fault_flag2*. (c) Torque, *x-y* subspace voltage, and *Fault_flag1* under $u_{xy\_max}$ = 4. (d) The misdiagnosis in dynamic process from 800 to 400 r/min. (e) Torque, *x-y* subspace voltage, and *Fault_flag1* under $u_{xy\_max}$ = 10. (f) The diagnosis results combined multi-variable. (g) The misdiagnosis in dynamic process from 3 to 0 N·m.

## VI. Conclusion and Foresight

Firstly, a clear comparison should be made between the natural fault-tolerant methods mentioned in the paper and those introduced in Section I to demonstrate the advantages of the current methods in certain application scenarios, as shown in Table II.

This paper introduces the *x-y* subspace open-loop FTC and fault diagnosis of SSPMSM. The specific research work is summarized as follows:

1) The VSD and double d-q models for SSPMSM with double neutral point topology are established respectively, and the relationship between them is obtained. Then, the expression of subspace current after winding open-circuit fault is analyzed.

2) By analyzing the torque component and harmonic component of the two sets of windings based on symmetric component method after the fault, the conflict in the closed-loop controller of the two subspaces is proved. A natural FTC method is designed. Different from the traditional FTC that pre-calculates the current reference value, this method can achieve excellent control performance without reconfiguring the controller after fault.

TABLE II
THE COMPARISON OF THE ADVANTAGES AND DISADVANTAGE OF NATURAL FAULT-TOLERANT METHODS

| Method | Ref. [14] | Ref. [15] | Ref. [16] | Ref. [17] | Ref. [18] | Proposed |
|---|---|---|---|---|---|---|
| Number of PI/PR controllers | 5 | 5 | 1 | 1 | 7 | 3 |
| Fault diagnosis | Needful | Needful | Needful | Needful | Needful | Needful |
| Fault location | Needless | Needless | Needless | Needful | Needless | Needless |
| Response speed | Medium | Slow | Slow | Slow | Medium | Fast |
| Copper loss | Low | Low | High | Low | High | Low |
| Torque pulsation | Low | Low | Low | High | Low | Low |

3) The two fault diagnosis algorithms based on *x-y* subspace voltage thresholds and current trajectories in the $\alpha$-$\beta$ subspace are introduced, and a fault diagnosis algorithm based on multi-variable joint diagnosis is proposed to improve the accuracy of the diagnosis results.

Finally, the proposed theoretical analysis is verified by corresponding experiments, which proves the correctness and operability of the theory. In addition, for the fault diagnosis strategy adopted in this paper, more accurate diagnostic algorithms can be further designed. Based on the establishment of a reliable and stable model, by adopting methods such as machine learning and designing fault diagnosis strategies, the algorithm can more effectively adapt to the motor control system and further enhance its robustness.

It should be noted that the FTC method introduced in this article aims to switch to the FTC algorithm after rapid diagnosis to ensure the dynamic performance from normal operation to fault operation. However, from both theoretical and experimental perspectives, we have concluded that the q-axis current after the fault contains a double-frequency component. Therefore, this will become one of the subsequent work contents.

## REFERENCES


[1] E. Levi, "Advances in Converter Control and Innovative Exploitation of Additional Degrees of Freedom for Multiphase Machines," *IEEE Trans. on Ind. Electron.*, vol. 63, no. 1, pp. 433–448, Jan. 2016.

[2] Z. L. Zhang, G. Z. Luo, and Z. B. Zhang *et al.*, "A Hybrid Diagnosis Method for Inverter Open-circuit Faults in PMSM Drives," *CES Trans. on Elect. Mach. and Syst.*, vol. 4, no. 3, pp. 180–189, Sept. 2020.

[3] F. Yu, W. Zhang, and Y. C. Shen *et al.*, "A Nine-phase Permanent Magnet Electric-drive-reconstructed Onboard Charger for Electric Vehicle," *IEEE Trans. on Energy Convers.*, vol. 33, no. 4, pp. 2091–2101, Dec. 2018.

[4] X. Liu, F. Yu, and J. F. Mao *et al.*, "Pre- and Post-fault Operations of Six-phase Electric-drive-reconstructed Onboard Charger for Electric Vehicles," *IEEE Trans. on Transport. Electrific.*, vol. 8, no. 2, pp. 1981–1993, Jun. 2022.

[5] Y. Q. Wei, M. Z. Qiao, and P. Zhu, "Fault-tolerant Operation of Five-phase Permanent Magnet Synchronous Motor with Independent Phase Driving Control," *CES Trans. on Elect. Mach. and Syst.*, vol. 6, no. 1, pp. 105–110, Mar. 2022.

[6] J. S. Wang, and G. H. Yang, "Data-driven Output-feedback Fault-tolerant Compensation Control for Digital PID Control Systems with Unknown Dynamics," *IEEE Trans. on Ind. Electron.*, vol. 63, no. 11, pp. 7029–7039, Nov. 2016.

[7] Q. Geng, Z. C. Li, and H. M. Wang *et al.*, "Natural Fault-tolerant Control with Minimum Copper Loss in Full Torque Operation Range for Dual Three-phase PMSM Under Open-circuit Fault," *IEEE Trans. on Power Electron.*, vol. 39, no. 1, pp. 1279–1291, Jan. 2024.

[8] X. Q. Wang, Z. Wang, and Z. X. Xu *et al.*, "Deadbeat Predictive Current Control-based Fault-tolerant Scheme for Dual Three-phase PMSM Drives," *IEEE J. of Emerg. and Sel. Topics in Power Electron.*, vol. 9, no. 2, pp. 1591–1604, Apr. 2021.

[9] F. Yu, M. Cheng, and F. Li *et al.*, "Fault Tolerant Control of Harmonic Injected Nine-phase Flux Switching Permanent Magnet Motor Drive System," in *Proc. of 2014 17th Int. Conf. on Elect. Mach. and Syst.*, Hangzhou, China, Oct. 2014, pp. 3117–3122.

[10] G. D. Feng, C. Y. Lai, and W. L. Li *et al.*, "Computation-efficient Solution to Open-phase Fault Tolerant Control of Dual Three-phase Interior PMSMs with Maximized Torque and Minimized Ripple," *IEEE Trans. on Power Electron.*, vol. 36, no. 4, pp. 4488–4499, Apr. 2021.

[11] G. D. Feng, Y. T. Lu, and C. Y. Lai *et al.*, "Fault Tolerant Maximum Torque Per Ampere (FT-MTPA) Control for Dual Three-phase Interior PMSMs Under Open-phase Fault," *IEEE Trans. on Ind. Electron.*, vol. 69, no. 12, pp. 12030–12041, Dec. 2022.

[12] F. Baneira, J. Doval-Gandoy, and A. G. Yepes *et al.*, "Control Strategy for Multiphase Drives with Minimum Losses in the Full Torque Operation Range Under Single Open-phase Fault," *IEEE Trans. on Power Electron.*, vol. 32, no. 8, pp. 6275–6285, Aug. 2017.

[13] J. W. Sun, Z. C. Liu, and Z. D. Zheng *et al.*, "An Online Global Fault-tolerant Control Strategy for Symmetrical Multiphase Machines with Minimum Losses in Full Torque Production Range," *IEEE Trans. on Power Electron.*, vol. 35, no. 3, pp. 2819–2830, Mar. 2020.

[14] I. G. Prieto, M. J. Duran, and P. Garcia-Entrambasaguas *et al.*, "Field-oriented Control of Multiphase Drives with Passive Fault Tolerance," *IEEE Trans. on Ind. Electron.*, vol. 67, no. 9, pp. 7228–7238, Sept. 2020.

[15] P. C. Shi, X. Q. Wang, and X. Meng *et al.*, "Adaptive Fault-tolerant Control for Open-circuit Faults in Dual Three-phase PMSM Drives," *IEEE Trans. on Power Electron.*, vol. 38, no. 3, pp. 3676–3688, Mar. 2023.

[16] J. Dai, X. L. Li, and W. B. Dai *et al.*, "Open-phase Natural Fault-tolerant Scheme based on Deadbeat Predictive Current Control for Symmetrical Six-phase Vernier PM Motor," *IEEE Trans. on Ind. Appl.*, vol. 61, no. 6, pp. 9337–9346, Nov.-Dec. 2025.

[17] V. F. M. B. Melo, G. F. da Paz, and I. S. de Freitas *et al.*, "Natural Fault-tolerant VV-DTC for Healthy and Postfault Operation of an Asymmetrical Six-phase Induction Machine Drive System with Single Neutral," *IEEE Trans. on Power Electron.*, vol. 39, no. 11, pp. 14398–14410, Nov. 2024.

[18] G. H. Yang, H. Hussain, and S. Li *et al.*, "Design and Analysis of Universal Natural Fault-tolerant SVPWM Strategy with Simplified Fault Diagnosis for Multiphase Motor Drives," *IEEE J. of Emerg. and Sel. Topics in Power Electron.*, vol. 11, no. 4, pp. 4340–4354, Aug. 2023.

[19] X. Q. Wang, H. W. Jiang, and P. C. Shi *et al.*, "Adaptive Fault-tolerant Control-based Fault Diagnosis of Dual Three-phase PMSM Drives," *IEEE J. of Emerg. and Sel. Topics in Power Electron.*, vol. 13, no. 2, pp. 2556–2564, Apr. 2025.

[20] L. H. Jin, X. Q. Wang, and Y. Mao *et al.*, "Online Attribute Matching based Few-sample Data-driven Diagnosis of Electrical Faults in PMSM Drive," *IEEE Trans. on Power Electron.*, vol. 39, no. 2, pp. 2620–2631, Feb. 2024.

**Aihua Liu** was born in Yancheng, China, in 2001. He received the B.Eng. degree in electrical engineering and automation in 2023 from the School of Electrical Engineering and Automation, Nantong University, Nantong, China, where he is currently working toward the M.Sc. degree in energy and power engineering.

His main research interests include electric-drive-reconstructed onboard charging system and its fault-tolerant control applied in electric vehicle.

**Feng Yu** (Member, IEEE) was born in Suzhou, China, in 1985. He received the B.Eng. degree in electrical engineering and automation from the School of Electrical Engineering, Sanjiang University, Nanjing, China, in 2008, the M.Sc. degree in electrical engineering from the School of Electrical and Information Engineering, Jiangsu University, Zhenjiang, China, in 2011, and the Ph.D. degree in the electrical engineering in the Department of Electrical Engineering, Southeast University, Nanjing, China, in 2016.

Since 2016, he has been with Nantong University, Nantong, China, where he is currently a professor in the School of Electrical Engineering and Automation. His current research interests include the control of multiphase machines and drives for applications ranging from automotive to renewable energy.

**Qingan Zhu** was born in Huainan, China, in 2002. He received the B.Eng. degree in electrical engineering and automation in 2024 from the School of Electrical Engineering and Automation, Nantong University, Nantong, China, where he is currently working toward the M.Sc. degree in control science and engineering.

His main research interests include power electronics and electric-drive-reutilized onboard charger along with its application in electric vehicle.

**Xiaoxin Wu** (Member, IEEE) was born in Nantong, China, in 1978. He received the B. Eng. degree in electric engineering and automation from the School of Automation, Nanjing University of Aeronautics and Astronautics, Nanjing, China, in 2000, and the M.Sc. and the Ph.D. degrees in electrical engineering from the School of Mechatronic Engineering and Automation, Shanghai University, Shanghai, China, in 2006 and in 2019,

Since 2000, he has been with Nantong University where he is currently an Associate Professor with the College of Electrical Engineering. His current major research interests include ac motor control, power electronic converters, and PWM converter/inverter systems.